Susceptibility of IN740 to HAZ Liquation Cracking and Ductility-Dip Cracking

The susceptibility of Ni-Cr-Co Alloy IN740 to heat-affected zone liquation cracking and ductility-dip cracking was evaluated and correlated to its solidification behavior

BY J. E. RAMIREZ

ABSTRACT

Evaluation of susceptibility to liquation cracking and ductility-dip cracking (DDC) of Alloy IN740 was conducted as part of the material selection criteria for application in ultrasupercritical (USC) boilers for power generation. The susceptibility to heat-affected zone (HAZ) liquation cracking and DDC was determined using Gleeble hot-ductility testing in the temperature range from 600° to about 1300°C and spot-Varestraint testing. The large on-cooling, nil-ductility range (NDR) of 229°C observed in Alloy IN740 indicates that the tested heat of this alloy is highly susceptible to liquation cracking in the HAZ. Welding conditions inducing shallower thermal gradients in the HAZ increase the size of the HAZ liquation cracking susceptibility region. Phase computational modeling indicates that segregation of B, Nb, and Si during solidification of Alloy IN740 results not only in the increase in the amount of low melting equilibrium phases such as MC and MB_2 but in the formation of low-melting, nonequilibrium phases such eta, Laves, and G phases. Therefore, the solidus temperature of the system is depressed to 1060°C. The resulting increase of the solidification range from 169.7° to 293.5°C of the Alloy IN740 heat tested explains the large NDR of 229°C observed in the alloy heat tested and its associated high susceptibility to HAZ liquation cracking. A pronounced loss or ductility dip was not observed in the Gleeble hot-ductility tested alloy heat in the temperature range from 600° to 1050°C. Therefore, Alloy IN740 is not susceptible to DDC cracking.

Introduction

In the 21st century, the world faces the critical challenge of providing abundant, cheap electricity to meet the needs of a growing global population while at the same time preserving the environment. Worldwide research and development efforts have been conducted in the last decades to develop and qualify high-temperature materials technology for ultrasupercritical boiler (USCB) power generation. The goal of the USCB programs is to increase boiler efficiencies and achieve lower emission levels. In the U.S.A., a program funded by the U.S. Department of Energy (DOE) and Ohio Coal Development Office (OCDO) has the goal to develop material technology capable of operating with steam temperatures of up to 732°C (1350°F) and pressures as high as 35 MPa (5000 lb/in.^{2}) (Ref. 1). These service conditions translate into higher hot gas path temperatures and the need for materials possessing the required strength, heat, and corrosion resistance for long-term, reliable service at higher temperatures. Additionally, the weldability of these base materials or ability to produce crack-free joints with acceptable mechanical properties is equally important as it has implications on original fabrication and repair.

A nickel-based alloy, Inconel® Alloy 740 (IN740) (Ref. 2), has been identified in the U.S.A. as a potential candidate for the severe operating conditions of USC boilers based on its resistance to fireside corrosion resistance, steamside oxidation, and good stress-rupture properties (Refs. 3–5). Alloy IN740 was developed as part of a similar program in Europe known as THERMIE. Alloy IN740 is a precipitation-hardenable, nickel-chromium-cobalt alloy with niobium, titanium, and aluminum additions. It is primarily strengthened through precipitation of gamma-prime phase (γ') and secondarily through the precipitation of carbides. Alloy 740 is a new alloy with no fabrication history that was derived from NIMONIC® Alloy 263. Therefore, the weldability of this new precipitation-hardenable alloy needed to be evaluated as part of the material selection criteria for application in USC boilers for power generation.

In general, nickel-based precipitation-hardenable alloys are susceptible to liquation cracking during welding and postweld heat treatment (PWHT) cracking, also known as reheat cracking or strain-age cracking, in the heat-affected zone (HAZ). Additionally, application of IN740 in the USC boilers requires wall thicknesses of up to 3 in. The high level of restraint in thick joints not only increases the susceptibility to liquation and PWHT cracking, but also makes the HAZ susceptible to ductility-dip cracking (DDC) during welding. Finally, the mechanical properties of Alloy IN740 welded joints are expected to depend on the "as-received" condition of the base metal, welding procedures, and pre- and postweld heat treatments.

The conducted evaluation of the weldability of Alloy IN740 included as follows: (1) HAZ liquation cracking susceptibility and HAZ DDC susceptibility as reported in this paper; (2) PWHT cracking susceptibility of Alloy IN740 and comparison with other common nickel-based precipitation-hardenable alloys such as IN718 and Waspaloy™; and (3) optimization of weldability or cracking resistance of Alloy IN740 as function of chemical composition along with mechanical properties of Gleeble-simulated HAZs of IN740 and full-sized IN740 welded plate joints in the postweld heat treated condition.

Liquation cracking is a high-temperature cracking phenomenon that occurs in

KEYWORDS

HAZ Liquation Cracking
Ductility-Dip Cracking (DDC)
Alloy IN740
Ultrasupercritical (USC) Boilers
Nil-Ductility Range (NDR)

J. E. RAMIREZ (jramirez@ewi.org) *is principal engineer, Edison Welding Institute, Columbus, Ohio.*

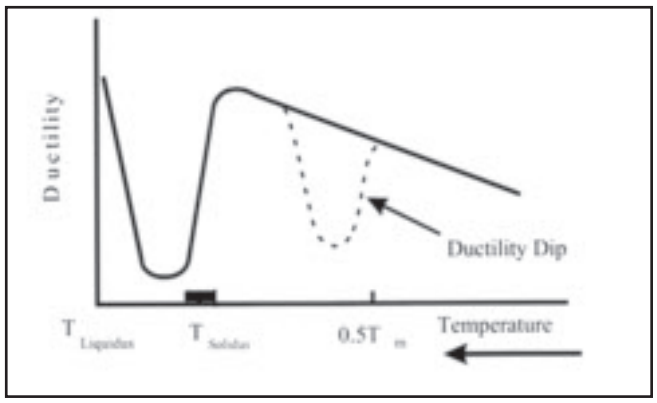

Fig. 1 — Schematic illustration of the temperature ranges where liquation cracking and DDC are observed in the HAZ of base metals during welding.

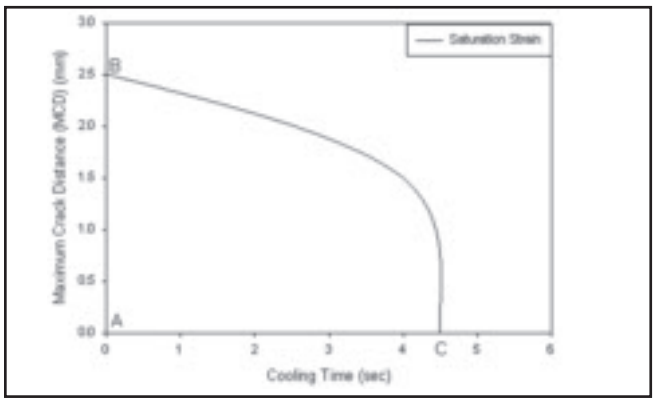

Fig. 2 — MCD as a function of cooling time using saturation strain during spot-Varestraint testing.

the HAZ region adjacent to the weld interface. This type of cracking is particularly prevalent in nickel- and aluminum-based alloys, plus fully austenitic stainless steels. The metallurgical basis for liquation cracking is the presence and persistence of liquid films at grain boundaries and the inability of those films to accommodate the thermally and/or mechanically induced strain experienced during weld cooling.

Ductility-dip cracking is a solid-state cracking that occurs intergranularly in weld metal and the HAZ. Although its exact mechanism has not been determined, it is associated with a ductility loss in the temperature range from one-half the absolute melting temperature up to the recrystallization or solidus temperature. This drop in elevated temperature ductility may occur either on heating to an elevated temperature or cooling from some peak temperature. Most of the materials susceptible to DDC are single phase from room temperature to the solidus temperature and tend to solidify as a face-centered cubic (FCC) single phase. In austenitic stainless steels and nickel-based alloys, there appears to be strong grain size dependence with coarser grain sizes promoting a higher susceptibility. Ductility-dip cracking is often associated with welding heavy sections commonly encountered in the power-generation industry. It has also been identified in other thermomechanical processes such as hot rolling and forging.

Figure 1 shows a schematic representation of the two temperature ranges in which low ductility is conducive to cracking during welding. Temperatures near to the solidus temperature and temperatures above half the melting temperature correspond to the temperature ranges where HAZ liquation cracking and HAZ DDC, respectively, can take place.

Materials and Experimental Procedures

Base Materials: The Alloy IN740 bar stock used for the weldability evaluation was initially melted using vacuum induction and subsequently electroslag remelted. The cylindrical cast (~21.0 in. in diameter) was then forged to 11.65 in. in diameter at 1180°C. The resulting 11.65-in.-diameter billet stock was then extruded at 1180°C to 3- × 6-in. bar. Finally, the bar was annealed at 1121°C (2050°F) and water quenched. A reannealing treatment of the bar at 1121°C for 3 h prior to water quenching was necessary due to high hardness in the as-produced bar. The provided material was identified as Heat BLT2819. The chemical composition of this heat of material is listed in Table 1.

Evaluation of HAZ Liquation Cracking Susceptibility: The susceptibility to HAZ liquation cracking of Alloy IN740 was determined using Gleeble hot-ductility testing and spot-Varestraint testing.

Gleeble Hot-Ductility Testing: The Gleeble hot-ductility test was used to characterize the ductility (reduction in area) of the material as function of temperature and to relate ductility recovery to HAZ liquation cracking susceptibility. Basically, small tensile samples were pulled to fracture rapidly in the vicinity of the solidus

Table 1 — Chemical Composition of Alloy IN740 (Heat BLT2819) Used for Testing

Element	C	Ni	Cr	Co	Nb	Ti	Al
Wt-%	0.029	Balance	24.4	20.0	2.0	1.8	1.0
Element	Si	Mn	P	S	Ag	B	Bi
Wt-%	0.53	0.26	<0.005	<0.001	<0.1	0.0045	<0.1
Element	Cu	Fe	Mo	Pb	V	Zn	Zr
Wt-%	0.02	0.45	0.50	0.6 ppm	<0.01	1 ppm	0.225

Table 2 — Conditions of Gleeble Hot-Ductility Testing of IN740 Alloy

Parameter	Description
On-Heating	
Test temperature	950°C and higher (1112°F and higher)
Heating rate to test temperature	111°C/s (200°F/s)
Holding time at test temperature	0.03 s
Stroke rate	5 cm/s (2 in./s)
Sample-free span (jaw spacing)	19 mm (0.75 in.)
Atmosphere	Argon
NST Determination	
Load	Just enough to overcome frictional force [≈20 kg (45 lb)]
Number of samples	3
On-Cooling	
Peak temperature	NST
Heating rate to peak temperature	111°C/s (200°F/s)
Holding time at peak temperature	0.03 s
Cooling rate to test temperature	40°C/s (72°F/s)
Holding time at test temperature	0.03 s
Stroke rate	5 cm/s (2 in./s)
Sample-free span (jaw spacing)	19 mm (0.75 in.)
Atmosphere	Argon

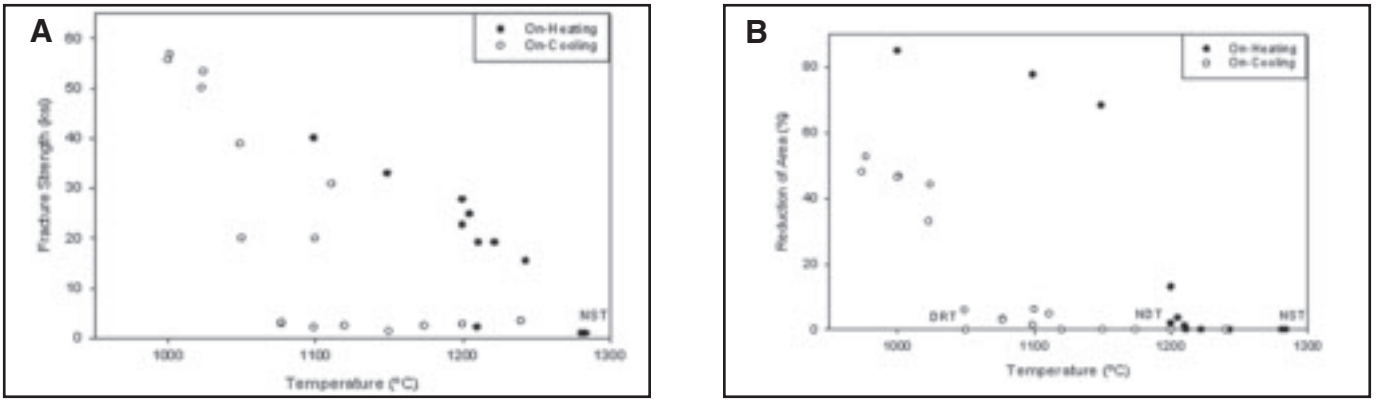

Fig. 3 — Gleeble hot-ductility of Alloy IN740 in the liquation cracking temperature range. A — Fracture strength; B — reduction of area as a function of testing temperature.

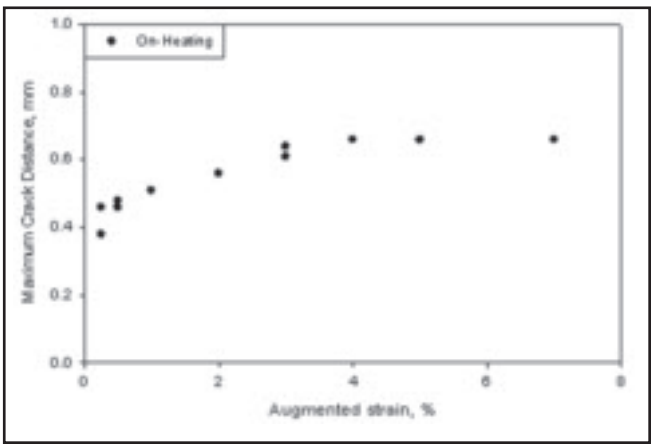

Fig. 4 — Spot-Varestraint testing results of IN740 during the on-heating part of the cycle.

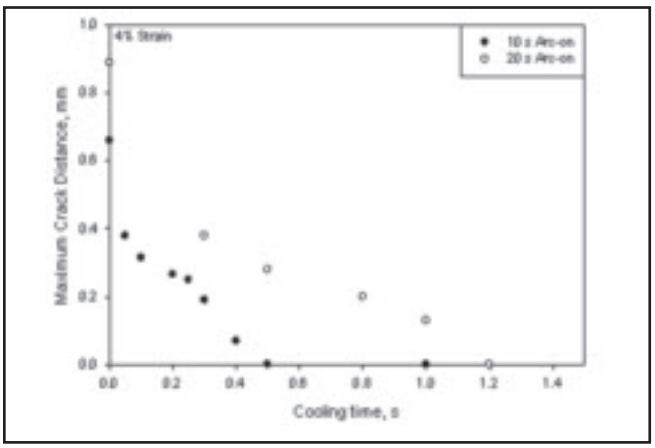

Fig. 5 — Comparison of the behavior of IN740 as a function of arc-on time of the spot-Varestraint testing.

temperature during the on-heating and on-cooling portion of a simulated weld thermal cycle in a Gleeble machine. The transverse reduction in area of the fracture samples was determined, thereby providing a measure of the ductility of the material at high temperature.

All testing was performed under an argon atmosphere using a Gleeble® 1000 system. After reaching a vacuum level of 40 millitorr, the chamber was backfilled with argon. The thermal cycles experienced by the samples during testing were measured using fine wire K-type thermocouples. These thermocouples were percussion welded to the samples. Immediately after the thermocouples were attached, the specimen was clamped between water-cooled jaws, which in addition to serving as grips, provide a means for introducing the current to the specimen for heating and ensuring a rapid cooling when the current flow is stopped.

The conditions for the Gleeble hot-ductility testing are given in Table 2. The testing temperatures were 950°C and higher. Standard specimens 6.35 mm in diameter and 100 mm long (0.25 × 4 in.) were used.

Spot-Varestraint Testing: The spot-Varestraint test was used to determine the size of the crack susceptibility region in the HAZ as function of welding conditions. During spot-Varestraint testing, a gas tungsten arc welding (GTAW) spot weld was produced in the center of a small specimen. After a predetermined weld time, the arc was extinguished and the specimen was forced to conform to the surface of a radiused die block. The strain imposed on the specimen was controlled through the radius of the die block and the thickness of the specimen. In this manner, HAZ liquation cracks were generated on the surface of the specimen adjacent to the GTA spot weld. The spot-Varestraint samples were 8 × 1.5 × 0.25 in. in size, and three spots were deposited in each specimen. The parameters used during spot-Varestraint testing of IN740 are listed in Table 3. The number of cracks and maximum crack distance (MCD) were measured in each sample as a function of augmented applied strain.

In order to evaluate the susceptibility to liquation cracking of IN740 during the on-heating and on-cooling parts of the thermal cycle, the cracking susceptibility envelope ABC as shown schematically in

Table 3 — Parameters Used during the Spot-Varestraint Testing

Parameter	Description
Welding process	GTAW, DCEN
Electrode	3/32-in. diameter, 2%Ce
Electrode preparation	30-deg included angle, 0.02-in. blunt
Electrode extension (beyond cup)	0.25 in. (6.35 mm)
Arc gap	0.080 in. (2.0 mm)
Voltage	11 ± 0.5 V
Current	150 ± 5 A
Arc-on time	10 and 20 s
Shielding gas	Argon at 30 ft^3/h
Shielding gas cup size	7
Bending rate	8 in./s
Hold time after bending	10 s
Spot diameter	11 mm

Fig. 2 was determined. This required the testing of specimens at different levels of strain and at zero cooling time (the time between arc extinction and specimen bending) until the saturation strain is reached (section AB of the envelope). The saturation strain is the strain above which the MCD remains constant. After that, specimens were tested using the saturation strain and different cooling times to determine the remaining part of the envelope (section BC). Section AB characterizes the susceptibility of the material during the on-heating part of the cycle. Section BC characterizes the susceptibility of the HAZ to cracking during the on-cooling part of the welding cycle.

Additionally, the effect of different welding conditions on the dimensional cracking susceptibility envelope was characterized by changing the arc-on time from 10 to 20 s during the on-cooling spot-Varestraint testing.

Evaluation of HAZ DDC Susceptibility: The susceptibility to HAZ DDC of IN740 was evaluated using Gleeble hot-ductility testing. The same procedure, specimen size, and geometry along with measurement of ductility as described for the Gleeble hot-ductility testing in the HAZ liquation cracking evaluation were used for the evaluation of DDC cracking. For DDC evaluation, the small tensile samples were fractured rapidly during the on-heating and on-cooling portions of a simulated weld thermal cycle in a Gleeble machine at specific temperatures in the 600° to 1000°C temperature range.

Experimental Results and Discussions

HAZ Liquation Cracking Susceptibility

Gleeble Hot-Ductility Testing: The results of the Gleeble hot-ductility testing of Alloy IN740 are listed in Table 4 and shown in Fig. 3. As part of the evaluation of the susceptibility to liquation cracking of Alloy IN740, the nil-ductility temperature (NDT), nil-strength temperature (NST), and ductility recovery temperature (DRT) were determined. As shown in Fig. 3B, the IN740 material loses all ductility when the testing temperature reaches 1205°C (NDT) on heating. The ductility remains low at higher temperatures and the fracture strength decreases to almost zero as the testing temperature is increased to 1280°C (NST), as shown in Fig. 3A. On cooling, after being exposed to a peak temperature, the alloy starts recovering ductility at 1050°C (DRT). Therefore, there are two temperature ranges within which the material exhibits negligible ductility (ND), the on-heating ND temperature range, and the on-cooling

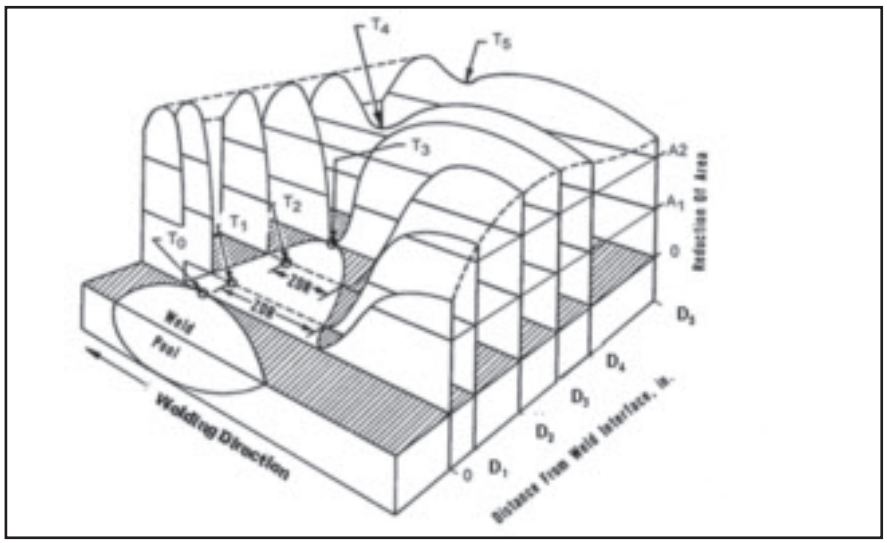

Fig. 6 — Schematic representation of the hot-ductility response of the HAZ.

Table 4 — Results of Hot-Ductility Testing during On-Heating and On-Cooling of IN740 Alloy in the Liquation Cracking Temperature Range

Specimen		Temperature (°C)		RA (%)	Fracture
Number	ID	Peak	Test		Strength (ksi)
HT-17[a]	HT950	–	952	82.2	60.3
HT-8	HT1000	–	1000	84.9	55.7
HT-1	HT1100	–	1099	77.7	40.0
HT-2	HT1150	–	1149	68.3	33.0
HT-3	HT1200	–	1200	13	27.7
HT-5	HT1200	–	1200	2	22.6
HT-6	HT1205	–	1205	3.6	24.8
HT-7	HT1210	–	1210	1.1	2.1
HT-4	HT1210	–	1211	0	19.1
HT-13	HT1220	–	1222	0	19.1
HT-14	HT1240	–	1243	0	15.4
NST-1	NST-1	–	1281	0	0.9
NST-2	NST-2	–	1282	0	0.9
NST-3	NST-3	–	1271	0	0.9
NST-4	NST-4	–	1284	0	0.9
CT-26[b]	CT1240	1272	1240	0	3.4
CT-22	CT1200	1271	1200	0	2.7
CT-23	CT1175	1271	1174	0	2.4
CT-17	CT1150	1271	1150	0	1.3
CT-18	CT1120	1268	1120	0	2.4
CT-25	CT1110	1272	1111	4.8	30.8
CT-16	CT1100	1271	1100	6.2	19.9
CT-19	CT1100	1272	1099	1.4	2.1
CT-28	CT1075	1273	1077	3.2	2.8
CT-29	CT1075	1273	1077	3.0	3.1
CT-15	CT1050	1271	1049	5.9	38.9
CT-20	CT1050	1268	1050	0	20.0
CT-24	CT1025	1272	1023	33.0	50.1
CT-27	CT1025	1272	1024	44.3	53.4
CT-1	CT1000	1267	999	11.5	2.1
CT-14	CT1000	1271	1001	46.7	56.8
CT-21	CT1000	1271	1000	46.4	55.7

(a) H: On-heating test specimens; T: Test temperature.
(b) C: On-cooling test temperature; T: Test temperature.

Table 5 — NST of the IN740 Alloy

Specimen	NST (°C)	Average NST (°C)
1	1281	
2	1282	
3	1271	1279.5
4	1284	

Table 6 — NDT, NST, and DRT Temperatures of IN740 Alloy

NDT (°C)	NST (°C)	DRT (°C)	(NDR) (°C)
1205	1279	1050	229

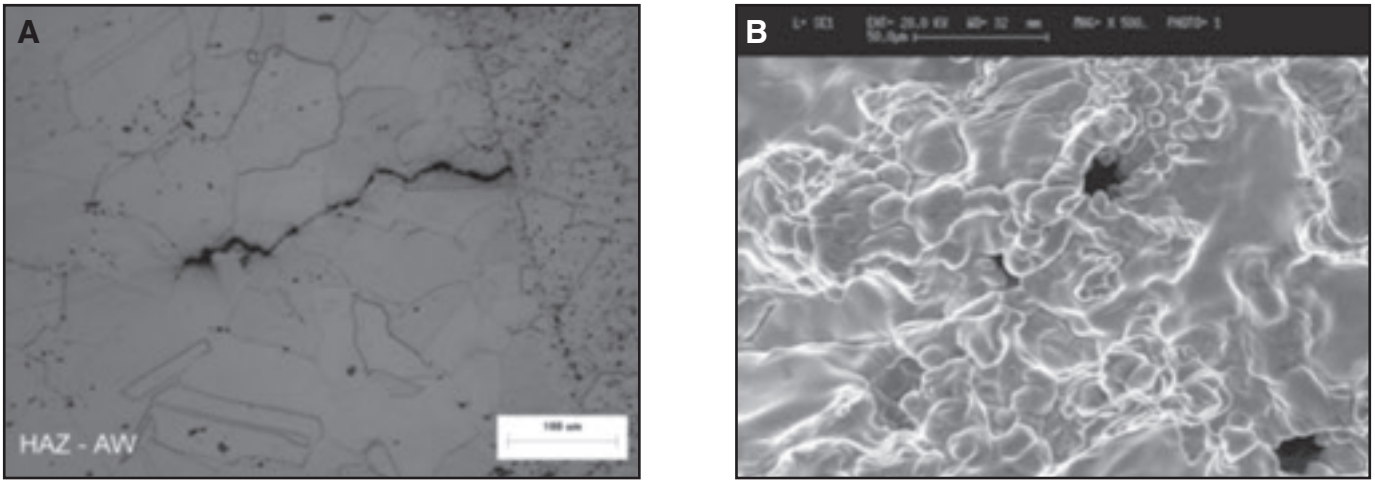

Fig. 7 — A — Example of microfissures observed in cross sections of the IN740 full-size welded joint; B — general fractographic characteristics of Gleeble on-cooling hot-ductility sample showing the presence of liquated phase remaining in the fracture surface.

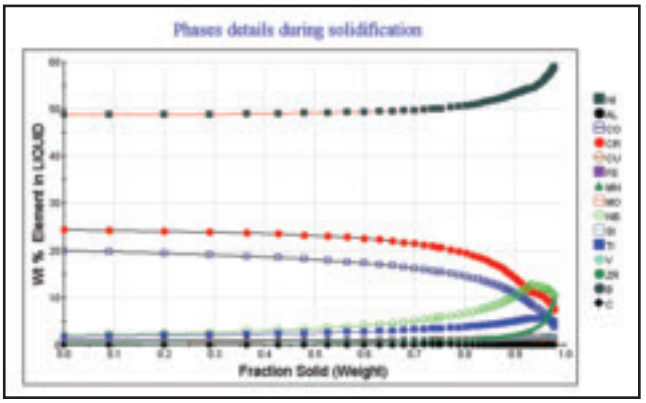

Fig. 8 — Predicted segregation of elements in the liquid as a function of the fraction solid.

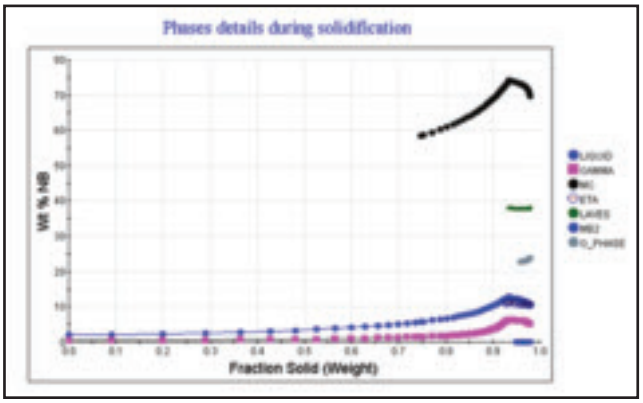

Fig. 9 — Predicted partitioning of Nb into different phases as function of the fraction solid.

ND temperature range.

The susceptibility to HAZ liquation cracking of Alloy IN740 was evaluated by using the on-cooling nil-ductility temperature range criteria (NDR). This is defined as the temperature difference between the peak temperature of the thermal cycle, which corresponds to the NST found during the on-heating portion of the simulated weld thermal cycle, and the on-cooling DRT, the temperature at which the ductility starts to recover after exposure to the NST.

Table 7 — Results of Spot-Varestraint Tests during the On-Heating Part of the Welding Cycle (0-s Cooling Time)

Sample ID	Augmented Strain (%)	Number of Cracks	MCD (mm)	Average MCD (mm)
0-0.25-1[a]	0.25	13	0.38	0.42
0-0.25-2	0.25	12	0.46	
0-0.5-1	0.5	19	0.48	0.47
0-0.5-2	0.5	20	0.46	
0-1-1	1	33	0.51	0.51
0-1-1	1	35	0.51	
0-2-1	2	39	0.56	0.56
0-2-2	2	38	0.56	
0-3-1	3	41	0.64	0.63
0-3-2	3	43	0.61	
0-4-1	4	45	0.66	0.66
0-4-2	4	44	0.66	
0-5-1	5	48	0.66	0.66
0-5-2	5	49	0.66	
0-7-1	7	54	0.66	0.66

(a) Cooling time – percent strain – specimen number.

The NDR indicates how fast the material recovers its ductility during cooling. A faster recovery of the ductility or smaller NDR indicates lower susceptibility to HAZ liquation cracking under similar welding conditions and, therefore, better weldability. The NST temperature obtained from different samples of Alloy IN740 are listed in Table 5. The NDT, NST, and DRT temperatures and the NDR determined for Alloy IN740 are listed in Table 6.

Spot-Varestraint Testing: The results of the spot-Varestraint testing during the on-heating part of the cycle are listed in Table 7 and shown in Fig. 4. The saturation strain for Alloy IN740 is about 4% as shown in Fig. 4. The maximum crack distance (MCD) was used as an index to characterize the size of the crack susceptibility region and, therefore, the susceptibility to liquation cracking. The MCD at saturation strain was about 0.66 mm. The results of the spot-Varestraint test during the on-cooling part of the cycle are listed in Table 8 and shown in Fig. 5.

The size of the crack susceptibility region determined by the spot-Varestraint testing is related to the NDR determined with the hot-ductility Gleeble testing, and

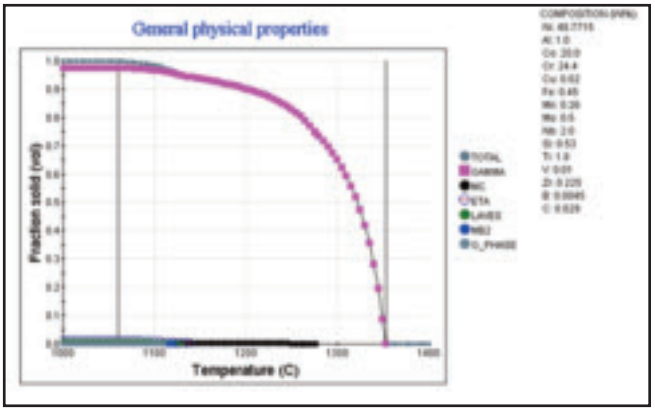

Fig. 10 — Predicted fraction of phases present in the solid as a function of temperature during solidification of the tested IN740 alloy heat.

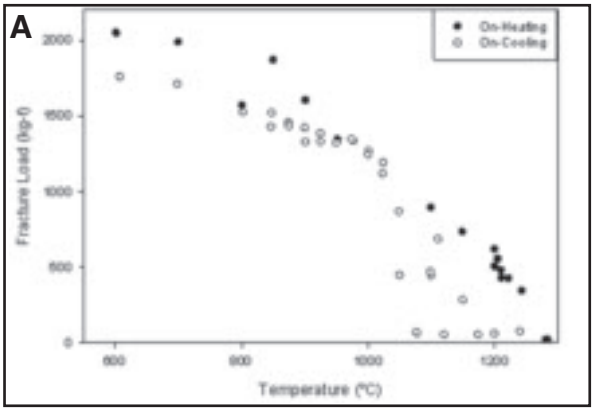

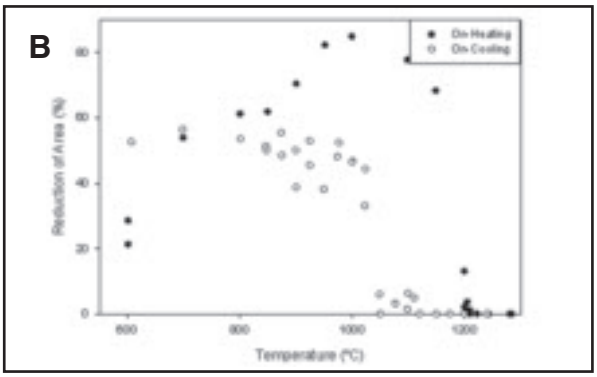

Fig. 11 — Gleeble hot-ductility tests of Alloy IN740. A — Fracture strength; B — reduction of area as a function of testing temperature.

their relationship depends on the temperature profile induced in the HAZ by the welding conditions. Figure 5 also shows the change in the size of the liquation cracking susceptibility envelope of IN740 as a function of the arc-on time. Increasing the arc-on time from 10 to 20 s increased the size of the susceptibility envelope by inducing a shallower thermal gradient in the HAZ, a wider HAZ, as compared to a shorter arc-on time condition. The same effect on the thermal gradient in the HAZ would be induced by increasing the heat input or by increasing preheat and/or interpass temperature during welding.

Discussion of Observed HAZ Liquation Behavior

Macroscopic Behavior: A schematic three-dimensional representation of the hot-ductility response of the HAZ of an alloy near the solidus temperature is shown in Fig. 6. Regions in the HAZ are initially heated and then cooled as the weld pool passes. The peak temperature will depend on the distance from the weld interface, decreasing as distance from the weld interface increases. For the conditions shown in Fig. 6, a point at a distance D4 from the weld interface will be heated to a peak temperature of T4 and shows no loss in ductility on heating or cooling. A point at a distance D3 from the weld interface will reach a peak temperature of T3. At this point in temperature, ductility drops to zero but recovers immediately on cooling. At a distance D2 from the weld interface, peak temperature is T2. However, ductility drops to zero on heating at T3 and does not return until a significant amount of cooling below T2 occurs. Closer to the weld interface, and consequently at higher peak temperature, the zero-ductility region (ZDR) becomes larger.

Additionally, during welding, material toward the front side of the weld pool is heated and expands, creating compressive stresses. As the weld pool moves in the welding direction, the material moving toward the back of the weld pool cools down and contracts, compressive stresses are relaxed, and tension stresses are developed. As illustrated in Fig. 6, adjacent to each moving weld pool there is a zero-ductility plateau. Therefore, the strain required to accommodate the generated tensile stresses may eventually reach

Table 8 — Results of Spot-Varestraint Tests during the On-Cooling Part of the Welding Cycle at Saturation Augmented Strain (4%)

Sample ID	Cooling Time (s)	Number of Cracks	MCD (mm)	Average MCD (mm)
		10-s Arc-on time		
0-4-1[(a)]	0	45	0.66	
0-4-2	0	44	0.66	0.66
0.05-4-1	0.05	42	0.38	
0.05-4-2	0.05	43	0.38	0.38
0.1-4-1	0.1	31	0.3	
0.1-4-2	0.1	38	0.33	0.315
0.2-4-1	0.2	26	0.25	
0.2-4-2	0.2	25	0.28	0.265
0.25-4-1	0.25	25	0.25	
0.25-4-2	0.25	22	0.25	0.25
0.3-4-1	0.3	21	0.13	
0.3-4-2	0.3	14	0.25	0.19
0.4-4-1	0.4	5	0.15	
0.4-4-2	0.4	0	0	0.07
0.5-4-1	0.5	0	0	
0.5-4-2	0.5	0	0	0.0
1-4-1	1.0	0	0	0
		20-s Arc-on time		
0-4-1	0	49	0.89	0.89
0.3-4-1	0.3	23	0.38	0.38
0.5-4-1	0.5	18	0.28	0.28
0.8-4-1	0.8	7	0.2	0.2
1.0-4-1	1.0	1	0.13	0.13
1.2-4-1	1.2	0	0	0

(a) Cooling time – percent strain – specimen number.

Table 9 — Comparison of the Susceptibility to Liquation Cracking of Different Alloys as Determined by the Gleeble Hot-Ductility Testing using the NDR Criteria

Alloy	NDT (°C)	NST (°C)	DRT (°C)	(NDR) (°C)
IN740 (Ref. 6)	1205	1279	1050	229
800H (Ref. 6)	–	1365	–	115
AC66 (Ref. 6)	–	1331	–	94
926 (Ref. 6)	–	1315	–	40
825 (Ref. 6)	–	1343	–	71
A-286 (Ref. 7)	1200	1350	1050	300
Type 310 (Ref. 7)	1325	1350	1325	25
Alloy 242 (annealed) (Ref. 8)	–	–	–	About 120
Alloy 242 (aged) (Ref. 8)	–	–	–	About 120
Waspaloy (different conditions) (Ref. 9)	1232–1253	1302–1330	1038–1204	52–232
IN718 (different conditions)(Ref. 9)	1190–1199	1272–1276	1149–1171	103–127
IN718 (different conditions)(Ref. 10)	1085–150	1283–1301	1010–1090	193–280

Table 10 — Phase Computational Modeling Predictions of Phase Transformation Characteristics of IN740 Alloy Heat BLT2819 in the Solidification Range (Based on Nominal Chemical Composition)

Temperature (°C)	Description
1353.5	Liquidus temperature (L)/start of solidification of gamma phase
1283.0	Start formation of MC carbides
1202.8	Start formation of MB_2 phase
1183.8	Solidus temperature (S)
169.7	Solidification range (L-S)

Temperature (°C)	Phase fraction (wt-%)			
	Gamma	MC	MB_2	Liquid
1183.8 (solidus)	99.78	0.22	0.01	–
1120.0 (annealing)	99.76	0.24	0.01	–
1205.0 (NDT)	98.76	0.2	–	1.04
1280.0 (NST)	86.8	0.03	–	13.17

Table 11 — Phase Computational Modeling Prediction of Segregation Behavior of Different Elements during Solidification of Alloy Heat BLT2819 (Based on Scheil-Gullier Solidification Model and 0.02 wt-% Liquid Fraction Solidification Cut-Off)

Element	Concentration in Liquid (wt-%)		Segregation Ratio (C_f/C_s)
	Start Solidification (C_s)	Finish Solidification (C_f)	
Ni	48.8	59.0	1.2
Cr	24.4	7.44	0.3
Co	20.0	3.8	0.19
Zr	0.225	9.82	43.6
Nb	2.0	10.71	5.36 (*)
Ti	1.8	4.94	2.7
Si	0.53	1.56	2.94 (*)
Mo	0.50	1.07	2.14
Mn	0.26	1.06	4.1
Al	1.0	0.76	0.76
Fe	0.45	0.18	0.4
B	0.0045	0.053	11.78 (*)
C	0.029	0.004	0.13

(*) Elements associated with liquation cracking behavior.

the strain capability of the HAZ. Hence, the susceptibility to liquation cracking of an alloy will increase with the size of the nil-ductility plateau.

The maximum size of the nil-ductility plateau of heat BLT2819 of Alloy IN740 is characterized by the on-cooling NDR (229°C) determined through the Gleeble hot-ductility testing and the MCD at saturation strain (0.66 mm) determined through the spot-Varestraint testing. The NDR and MCD represent the temperature difference and distance, respectively, between the isotherms and location of the weld interface and the tip of the liquation cracks in the HAZ. The large NDR of about 230°C observed in Alloy IN740 indicates that this alloy is highly susceptible to liquation cracking in the HAZ. Table 9 shows a comparison of the susceptibility to liquation cracking of different alloys determined by Gleeble hot-ductility testing based on the NDR criteria as reported in the literature (Refs. 6–10).

The actual size of the dimensional envelope of the nil-ductility plateau observed in the HAZ of a particular material depends on the thermal profile induced by welding conditions (heat input, preheat, etc.), as shown in Fig. 5 for Alloy IN740. Welding conditions creating a shallower thermal profile will increase the size of the cracks (nil-ductility enveloped) as the distance between the isotherms of the weld interface and the tip of the liquation cracks in the HAZ will increase.

Reported welding field testing of IN740 (Ref. 11) indicates the use of different combinations of welding processes including pulsed gas metal arc welding (P-GMAW) and cold- and hot-wire GTAW, shielding gases like argon and argon-helium mixtures, welding wires, heat inputs, single-V and U-narrow groove joint bevel designs, number of weld passes to complete the joint by changing the bead size, and plate thicknesses up to 1.0 in. to develop and optimize the welding procedures. Even though some of those welding procedures showed promising results in thin-walled applications, most of the welding techniques that were tested resulted in some degree of liquation cracking in the HAZ of Alloy IN740, as shown in Fig. 7. Additionally, variation of the degree of cracking or number of microfissures present in the welded joints from heat to heat of Alloy IN740 was also reported.

The reported welding results confirms the high susceptibility to HAZ liquation cracking of heat BLT2819 as determined by Gleeble hot-ductility and spot-Varestraint testing. Additionally, it also indicates that if an alloy such as IN740 is very susceptible to HAZ liquation cracking, the window of opportunity to develop a robust welding procedure that allows a normal welding parameter variation found in a production environment without inducing HAZ liquation cracking is very limited. Therefore, a better understanding of the fundamental causes of the observed liquation cracking susceptibility of Alloy IN740 is of outmost importance and further analysis of the solidification behavior of Alloy IN740 was conducted.

Microscopic Behavior: Liquid metal is invariably associated with the HAZ because the HAZ stretches from the base metal to the edge of the fusion zone and

will include all or part of the mushy zone. However, the mushy zone liquid generally does not contribute to poor weldability, because during the normal course of solidification, it is always open to the fusion zone. The fusion zone acts as a source of liquid to backfill or heal the shrinkage or cracks that might form.

However, phases that form during casting or processing of the alloy such as MC carbides and Laves phases have the potential to initiate melting by constitutional liquation or equilibrium melting in the HAZ on-heating during welding and spread along the grain boundaries (Refs. 12–14). Constitutional liquation can occur below the system solidus and be located away from the HAZ mushy zone. Additionally, the liquation of MC carbides may produce such great local solute enrichment at the grain boundary that the resolidification of these boundaries can be greatly delayed, increasing the nil-ductility plateau size, which increases the chances of HAZ liquation cracking.

Anything that increases the life of the intergranular liquid relative to the onset of residual tensile stresses accentuates liquation cracking. Additionally, chemical segregation at grain boundaries can also promote grain boundary liquation where melting or resolidification of equilibrium phases is controlled by their equilibrium solidus temperature (Refs. 12, 15, 16).

Therefore, in order to gain understanding of the solidification behavior of Alloy IN740 and identify the factors that control the high susceptibility to liquation cracking observed in heat BLT2819, phase computational modeling was used to predict the formation of thermodynamic stable phases as well as segregation of elements, partition of elements, and phase transformations during solidification.

Table 10 lists the thermodynamic stable phase transformation characteristics of heat BLT2819 predicted by computational modeling based on nominal chemical composition. The model predictions indicate a solidus and liquidus temperature equal to 1183.8° and 1353.5°C, respectively, and the formation of MC and MB_2 as stable phases. Taking into account that the tested alloy heat was processed under a controlled condition and it was annealed twice before testing, it can be assumed that the degree of segregation present in the as-received material was low and the behavior during the on-heating part of the welding cycle is controlled by thermodynamically stable phases present in the material. The solution-annealed heat treatment cleans the grain boundary of residual elements and dissolves small particles available for constitutional liquation, reducing the potential for liquation cracking (Ref. 15). The results of computational modeling pointed out that at 1205°C (NDT of the tested alloy heat), the alloy consists of about 98.67 wt-% gamma phase, 0.2 % MC, and 1.04% liquid phase. This suggests that the NDT of the alloy corresponds to the temperature where liquid starts to form at the grain boundaries during heating. At 1280°C (NST of the alloy heat), 86.8 wt-% gamma phase, 0.03% MC, and 13.17% liquid are present in the material. Therefore, these results indicate that the NST of the material during heating corresponds to the temperature where most of the stable second phases are dissolved and the amount of liquid phase is enough to envelop most of the grain, which results in almost zero strength of the material.

On the other hand, the DRT (1050°C) determined during cooling of the tested heat is much lower than the solidus temperature of 1183.8°C predicted by the computational model. Therefore, a different condition needed to be considered to explain the behavior observed during the on-cooling part of the testing. The additional modeling was conducted to evaluate segregation of elements, partitioning of some elements, and phase transformations during solidification on cooling. Solidification was modeled based on the Scheil-Gulliver approach, and a 0.02 wt-% liquid fraction solidification cutoff was assumed.

Table 12 — Phase Computational Modeling Prediction of Partitioning Behavior of Different Elements during Solidification of Alloy Heat BLT2819 (Based on Scheil-Gullier Solidification Model and 0.02 wt-% Liquid Fraction Solidification Cut-Off)

Element	Phase	Concentration (wt-%)	Fraction Solid Range (wt-%)
B	MB_2	31.0	0.95–0.98
	Liquid	0.053	0.98
Nb	MC	58.0–70.0	0.75–0.98
	Laves	38.0	0.93–0.98
	G-Phase	24.0	0.96–0.98
	Liquid	11.0	0.98
Si	G-phase	12.0	0.96–0.98
	Laves	4.5	0.93–0.98
	Liquid	1.6	0.98

Table 13 — Phase Computational Modeling Predictions of Phase Transformation Characteristics of IN740 Alloy Heat BLT2819 in the Solidification Range (Based on Scheil-Gullier Solidification Model and 0.02 wt-% Liquid Fraction Solidification Cut-Off)

Temperature (°C)	Description
1353.5	Liquidus temperature (L) and start of solidification of gamma phase
1276.0	Start formation of MC carbides
1140.0	Start formation of Eta phase
1130.0	Start formation of Laves phase
1120.0	Start formation of MB_2 phase
1110.0	Start formation of G-phase
1060.0	Solidus temperature (S)
293.5	Solidification range (L-S)

Temperature (°C)	Phase fraction (Vol-%)			
	Gamma	MC	Eta/Laves	MB_2/G
1060.0 (S)	97.3	0.3	1.2/1.0	0.1/0.1

Figure 8 shows the predicted evolution of segregation of different elements on the liquid phase as solidification progresses. Table 11 lists the predicted degree of segregation of different elements in the liquid phase from the start of solidification (C_s) to the completion of solidification (C_f), as characterized by a segregation ratio (C_f/C_s). Alloying elements that experience a large degree of segregation during solidification of Alloy IN740 in decreasing order of the corresponding segregation ratio include zirconium, boron, niobium, manganese, and silicon. It is important to indicate that sulfur, which may depress the melting point of microstructural constituents like Laves phases (Ref. 15), is not included in the databases that support the computational model used. Of these elements, boron, niobium, and silicon are normally associated with the susceptibility to liquation cracking by increasing the solidification range or modifying the surface tension of the liquid phase and its ability to wet the grain boundaries (Refs. 12, 13, 17–22).

The partitioning of these three elements was evaluated as a function of the advancement of the solidification front. Table 12 describes the partitioning of B, Nb, and Si between the different phases, in addition to the gamma phase, as the IN740 solidifies. Boron partitions mainly between MB_2

Table 14 — Results of Hot-Ductility Testing during On-Heating and On-Cooling of IN740 Alloy, in the DDC Temperature Range

Specimen Number	ID	Temperature °C Peak	Test	RA (%)	Fracture Strength (ksi)
HT-15[a]	HT600	–	602	21.2[c]	92.0
HT-12	HT600	–	602	28.5[c]	91.7
HT-11	HT700	–	700	53.9	89.1
HT-10	HT800	–	801	61.2	70.4
HT-16	HT850	–	850	61.8	83.9
HT-9	HT900	–	901	70.4	71.9
HT-17	HT950	–	952	82.2	60.3
HT-8	HT1000	–	1000	84.9	55.7
CT-1	CT1000	1267	999	11.5	2.1
CT-14	CT1000	1271	1001	46.7	56.8
CT-21	CT1000	1271	1000	46.4	55.7
CT-30	CT975	1268	977	52.7	59.9
CT-31	CT975	1271	974	48.1	60.3
CT-2	CT950	1275	953	3.8	10.8
CT-3	CT950	1273	952	2.9	10.9
CT12[b]	CT950	1271	950	38.1	59.3
CT-32	CT925	1272	925	52.9	59.6
CT-33	CT925	1270	925	45.4	62.1
CT-4	CT900	1270	900	0	3.2
CT-9	CT900	1272	901	38.7	59.5
CT-10	CT900	1270	901	4	3.1
CT-11[b]	CT900	1271	900	50	63.7
CT-34	CT875	1271	874	55.4	65.4
CT-35	CT875	1272	875	48.4	64.3
CT-5	CT850	1270	847	51.2	64.0
CT-13	CT850	1270	848	50.0	68.1
CT-6	CT800	1271	802	53.5	68.3
CT-7	CT700	1270	699	56.4	76.7
CT-8	CT600	1272	608	52.6[c]	78.8

(a) H: On-heating test specimens; T: Test temperature.
(b) C: On-cooling test temperature; T: Test temperature.
(c) These samples did not break during testing. Therefore, the actual reduction of area at fracture is higher than indicated.

phase and the remaining liquid phase during the late stages of solidification (0.95 to 0.98 fraction solid range). Niobium partitions to MC carbides starting at about 0.75 fraction solid range while Nb and Si partition into Laves, G phases, and remaining liquid toward the end of the solidification process (0.93 to 0.98 fraction solid range). Figure 9 shows the predicted partitioning behavior of Nb during solidification as function of fraction solid.

Segregation during solidification of Alloy IN740 causes not only the amount of low melting equilibrium phases such as MC and MB_2 to increase but the formation of low melting nonequilibrium phases such as eta, Laves, and G phases, as listed in Table 13. Figure 10 shows the predicted fraction of phases present in the solid as a function of temperature during solidification. In this system, the sequence of solidification during cooling seems to be as follows:

$$L \rightarrow L + \gamma \rightarrow L + \gamma + MC \rightarrow L + \gamma + MC + \text{Eta phase} \rightarrow L + \gamma + MC + \text{Eta phase} + \text{Laves phase} \rightarrow L + \gamma + MC + \text{Eta phase} + \text{Laves phase} + MB_2 \rightarrow L + \gamma + MC + \text{Eta phase} + \text{Laves phase} + MB_2 + \text{G phase}.$$

As a result, the solidus temperature of the system is depressed to 1060°C, which is close to the DRT (1050°C) observed for the tested alloy heat. Therefore, the segregation of boron, niobium, and silicon during solidification results in the increase of the solidification range from 169.7° to 293.5°C of the IN740 alloy heat tested. This result explains the large nil-ductility range (NDR) of 229°C observed in the alloy heat tested and its associated high susceptibility to HAZ liquation cracking.

Experimental Results of HAZ DDC Susceptibility of Alloy IN740

The results of the Gleeble hot-ductility testing of Alloy IN740 in the DDC temperature range are listed in Table 14 and shown in Fig. 11. Figure 11 shows the general hot-ductility behavior of Alloy IN740 in the temperature range between 600° and 1300°C. The actual ductility of the samples tested on-heating at 600°C is higher than indicated in Fig. 11 because the samples did not fracture at the maximum displacement programmed for the testing. The general trend of the data shown in Fig. 11 indicates that during the on-cooling part of the welding thermal cycle, the strength and ductility of the alloy start to recover and continually increase as it cools down from 1050° to 600°C. A pronounced loss or ductility dip was not observed in the tested alloy heat. Therefore, the results of the Gleeble hot-ductility testing of Alloy IN740 indicate that this alloy heat is not susceptible to DDC cracking.

Conclusions and Recommendations

- On-heating, Alloy IN740 (Heat BLT2819) showed a nil-ductility tests temperature (NDT) and nil-strength temperature (NST) equal to 1205° and 1280°C, respectively. On cooling, after experiencing a peak temperature equal to the NST, the alloy starts recovering ductility at 1050°C (DRT).
- Alloy IN740 (Heat BLT2819) showed an on-cooling nil-ductility temperature range (NDR) of about 230°C. This large NDR indicates that Alloy IN740 is highly susceptible to HAZ liquation cracking.
- Under spot-Varestraint testing, the saturation strain for Alloy IN740 is about 4% and the maximum crack distance (MCD) at saturation strain was about 0.66 mm. As expected, increasing the arc-on time from 10 to 20 s increased the size of the HAZ liquation cracking susceptibility envelope.
- Phase computational modeling, based on nominal chemical composition of heat BLT2819, predicts a solidus and liquidus temperature equal to 1183.8° and 1353.5°C, respectively, and the formation of MC and MB_2 as stable phases. At 1205°C (NDT) and 1280°C (NST) about 1.0 and 13.2 wt-% liquid, respectively, is predicted to be present. Therefore, NDT and NST may correspond to the initiation of liquation and to the presence of enough liquid to surround the grains, respectively, on heating. The predicted liquidus temperature (1183.8°C) is much higher than the DRT (1050°C) observed on-cooling.
- Phase computational modeling of solidification of Alloy IN740, based on the Scheil-Gulliver approach and a 0.02 wt-% liquid fraction solidification cut-off, predicts segregation ratios for zirconium, boron, niobium, manganese, and silicon ranging from 44 to 2. Boron, niobium, and silicon tend to partition to MB_2, MC, Laves, G phase, and remaining liquid during the last stages of solidification.
- Segregation during solidification of Alloy IN740 results not only in the increase in the amount of low melting equilibrium phases such as MC and MB_2 but in the formation of low melting nonequilibrium phases such as eta, Laves, and G phases. Therefore, the solidus temperature of the system is depressed to 1060°C, which is close to the DRT (1050°C) observed for the tested alloy heat.
- The segregation of boron, niobium, and silicon during solidification results in the increase of the solidification range from

169.7° to 293.5°C of the Alloy IN740 heat tested, which explains the large nil-ductility range (NDR) of 229°C observed in the alloy heat tested and its associated high susceptibility to HAZ liquation cracking.

• A pronounced loss or ductility dip was not observed in the Gleeble hot-ductility tested alloy heat in the temperature range from 600° to 1050°C. Therefore, Alloy IN740 is not susceptible to DDC cracking.

Acknowledgments

This publication was prepared with support of the U.S. Department of Energy, under Award No. DE-FG26-01NT41175 and the Ohio Coal Development Office of the Ohio Department of Development under Grant Agreement Number CDO/D-0020 (now D-05-02A). However, any opinions, findings, conclusions, or recommendations expressed herein are those of the author(s) and do not necessarily reflect the views of the DOE and/or the Ohio Coal Development Office of the Ohio Department of Development.

References

1. Viswanathan, R., Purgert, R., Goodstine, S., Tanzosh, J., Stanko, G., Shingledecker, J. P., and Vitalis, B. 2008. U.S. program on materials technology for ultracritical coal-fired boilers. *Proceedings of the 5th International Conference on Advances in Materials Technology for Fossil Power Plants*. ASM International, pp. 1–15.

2. Inconel® Alloy 740 product data sheet. Special Metals Corp., September 2004.

3. Purgert, R., Rawls, P., and Viswanathan, R. 2008. Coal-fired power materials. *Advanced Materials and Processes*, pp. 47–49.

4. Gagliano, M. S., Hack, H., and Stanko, G. 2009. Update on the fireside corrosion resistance of proposed advanced ultrasupercritical superheater and reheater materials: Laboratory and field test results. *Clearwater Coal Conference, 34th International Technical Conference on Coal Utilization and Fuel Systems*. Clearwater, Fla.

5. Sarver, J. M., and Tanzosh, J. M. 2007. The steamside oxidation behavior of candidate USC materials at temperatures between 650°C and 800°C. *5th International Conference on Advances in Materials Technology for Fossil Power Plants*. Marco Island, Fla.

6. Wilken, K. 1999. Investigation to compare hot cracking tests — externally loaded specimens. *IIW Doc.: IX-1945-99*.

7. Lin, W., Lippold, J. C., and Baeslack III, W. A. 1993. An evaluation of heat-affected zone liquation cracking susceptibility, Part I: Development of a method for qualification. *Welding Journal* 72(4): 135-s to 153-s.

8. Maguire, M. C., and Headley, T. J. 1990. A weldability study of Haynes Alloy 242. *Proceedings of Symposium on Weldability of Materials*. Detroit, Mich.

9. Qian, M. 2001. An investigation of the repair weldability of Waspaloy and Alloy 718. PhD thesis, OSU.

10. Lu, Q., Lippold, J. C., and Bowers, R. J. 2001. Alloy 718 heat-affected zone microstructural evolution after multiple repair and postweld heat-treatment cycles. EWI Report MR0111.

11. Sanders, J. M., Ramirez, J. E., and Baker, B. A. 2008. Weldability investigation of Inconel® Alloy 740 for ultrasupercritical boiler applications. *Proceedings of the 5th International Conference on Advances in Materials Technology for Fossil Power Plants*. ASM International, pp. 818–829.

12. Lundin, C. D., and Qiao, C. Y. P. 1992. Evaluation of HAZ liquation cracking susceptibility and HAZ softening behavior in modified 800H. *NIST Report DE93004064*, pp. 1–114.

13. Woo, I., Nishomoto, K., Tanaka, K., and Shirai, M. 2000. Characteristics of heat affected zone cracking in Inconel 718 cast alloy. *Welding International* 14(05): 19–28.

14. Woo, I., Nishomoto, K., Tanaka, K., and Shirai, M. 2000. Effect of grain size on heat affected zone cracking susceptibility. *Welding International* 14(07): 9–17.

15. Woo, I., Nishomoto, K., Tanaka, K., and Shirai, M. 2000. Effect of homogenization heat treatment on heat affected zone cracking susceptibility. *Welding International* 14(07): 25–34.

16. Nishimoto, K., Woo, I., and Shirai, M. 1965. Effect of cerium addition on hot cracking susceptibility in HAZ of cast Alloy 718. *IIW Doc. IX-1965-00*, pp. 1–15.

17. Lippold, J. C. 1984. An investigation of weld cracking in Alloy 800. *Welding Journal* 63(3): 91-s to 103-s.

18. Wu, K. C., and Herfert, R. E. 1967. Microstructural studies of Rene 41 simulated weld heat-affected zones. *Welding Journal* 46(1): 32-s to 38-s.

19. Lu, Q. 1999. HAZ microstructural evolution in Alloy 718 after multiple repair and PWHT cycles. PhD dissertation, OSU.

20. DuPont, J. N., and Robino, C. V. 1999. The influence of Nb and C on the solidification microstructure of Fe-Ni-Cr alloys. *Scripta Materialia* 41(4): 449–454.

21. DuPont, J. N., Robino, C. V., and Marder, A. R. 1998. Solidification and weldability of Nb-bearing superalloys. *Welding Journal* 77(10): 417-s to 431-s.

22. Shi, S., Lippold, J. C., and Ramirez, J. 2010. Hot ductility behavior and repair weldability of service-aged, heat-resistant stainless steel castings. *Welding Journal* 89(10): 210-s to 217-s.